Received: 19 January 2022 | Revised: 18 February 2022 | Accepted: 28 February 2022

DOI: 10.1002/agt2.194

Aggregate Open Access WILEY

RESEARCH ARTICLE

Therapeutic dendritic cell vaccines engineered with antigen-biomineralized Bi_2S_3 nanoparticles for personalized tumor radioimmunotherapy

Huan Yu[1] | **Haoxiang Guo**[1] | **He Zu**[1] | **Heng Ding**[1] | **Subin Lin**[2] | **Yangyun Wang**[1] | **Leshuai W Zhang**[1] | **Yong Wang**[1]

[1]State Key Laboratory of Radiation Medicine and Protection, School of Radiation Medicine and Protection, Collaborative Innovation Center of Radiation Medicine of Jiangsu Higher Education Institutions, Soochow University, Suzhou, China

[2]Department of Orthopedic, The Second Affiliated Hospital of Soochow University, Suzhou, China

Correspondence
Yong Wang and Leshuai W Zhang, State Key Laboratory of Radiation Medicine and Protection, School of Radiation Medicine and Protection, Collaborative Innovation Center of Radiation Medicine of Jiangsu Higher Education Institutions, Soochow University, Suzhou 215123, China.
Email: yongwang@suda.edu.cn; zhangls@suda.edu.cn

Funding information
National Natural Science Foundation of China, Grant/Award Numbers: 22122407, 12175162, 32171403, 12075164, 31971319, 21874097; National Key Research Program of China, Grant/Award Number: 2018YFA0208800; Tang Scholar Program; Scientific Research Program for Young Talents of China National Nuclear Corporation and A Priority Academic Program Development of Jiangsu Higher Education Institutions

Abstract

Therapeutic vaccines, an exciting development in cancer immunotherapy, share the goal of priming of personalized antigen-specific T-cell response by precise antigen presentation of dendritic cells (DCs), but major obstacles include insufficient antigen loading and off-target to DCs remain to their success. Here, we developed an imageable therapeutic vaccine with whole-antigen loading and target delivery constructed by ovalbumin (OVA)-biomineralized Bi_2S_3 nanoparticles-pulsed DCs. Relying on the strong X-ray absorption and fluorescence labeling performance of Bi_2S_3@OVA nanoparticles, the in vivo spatiotemporal fate of the vaccine (Bi_2S_3@OVA@DC) can be noninvasively monitored by computed tomography and near-infrared fluorescence imaging in real time. The Bi_2S_3@OVA@DC can rapidly and durably accumulate in draining lymph nodes and thus trigger stronger T-cell responses compared to OVA-pulsed DCs. Meanwhile, Bi_2S_3@OVA@DC can further achieve in vivo antitumor effects against OVA-expressing B16F10 melanoma when combined with fractionated radiotherapy, resulting from the upregulation of cytotoxic $CD8^+$ T cells and restraint of regulatory T cells in the tumor microenvironment, and the systemical secretion of OVA-specific IgG1/IgG2α antibody. Overall, we successfully fabricated an engineered DC vaccine featured in high whole-antigen loading capacity that can be precisely delivered to the lymphatic system for visualization, serving as a powerful therapeutic platform for cancer radioimmunotherapy.

KEYWORDS

antigen-biomineralized Bi_2S_3 nanoparticles, dendritic cells, radioimmunotherapy, therapeutic vaccines, visualization

1 | INTRODUCTION

Tumor vaccines are efficiently recognized and responded to by the host immune system, causing a systemic immune response for tumor elimination.[1,2] Typically, therapeutic tumor vaccines can minimize metastasis and prevent recurrence through training the innate immune system to obtain long-acting tumor antigen-specific killing capacity, thereby significantly improving the prognosis of patients.[3,4] As a unique milestone, Sipuleucel-T (Provenge®) vaccine has been approved by US FDA to enter the market for the treatment of metastatic prostate cancer.[5] Provenge® is a pioneer in cell therapy that offers dendritic cells (DCs) targeted immune response and improves median survival for some patients.[6] However, therapeutic DCs are engineered in vitro before administration and may be difficult to retain DCs mature phenotype continuously after infusion, leading to insufficient antigen expression and presentation.[7] These could be the main reasons for the low clinical response rate. Recent studies show that the addition of adjuvants can improve the poor immunogenicity of tumor vaccines and generate a robust antitumor immune response.[8] Although approved vaccines are generally made by mixing soluble and particulate antigens with adjuvants to elicit immune

responses, the immune-stimulating and long-lasting effect of traditional vaccines remain to be explored.[9]

Nanotechnology has opened a window to offer unique advantages for the development of cancer vaccines.[10,11] Nanoparticles can impart more stability with high antigen loading and less peptide degradation of antigenic subunits, thereby increasing the systemic exposure time of the antigenic peptides, which in turn produces an improved antitumor response.[12] Furthermore, nanoparticles can be used as a codelivery system for encapsulating antigen and adjuvant, generating potent immune responses with promising antitumor efficacy.[13-15] For example, Moon et al. developed a personalized cancer vaccine delivery platform based on self-assembling nanoparticles that can codeliver peptide antigens and adjuvants to potentiate antigen-specific immune responses.[16,17] Whereas, these noncellular particles as nanovaccines have low efficiency in migrating to lymph nodes (LNs) or targeting DCs.[18,19] Alternatively, DCs loaded with nanovaccines may provide an excellent cell platform for nanoparticle targeting immune organs.[20] It is worth mentioning that tracing and monitoring of nanovaccine-loaded DCs after infusion into the body is the key to optimizing the timing and dose of administration, aiming to enhance the immune response.[21,22] There have been many types of multifunctional nanoparticles that may help investigate the immunotherapeutic effects with associated mechanisms.[23,24] For real-time visualization of immune cells, nanoparticle-mediated computed tomography (CT) imaging has more unique advantages compared to radionuclide imaging, which needs freshly radionuclide-labeled biologics/chemicals that are complicated and time consuming to prepare.[25,26] In our previous work, we have prepared the Bi_2S_3 nanoparticles with a CT contrast potential through the one-step protein-mediated biomimetic mineraliztion process.[27] Therefore, it is promising that DCs loaded antigen-biomimetic Bi_2S_3 nanoparticles may play a robust immune role as a new generation of nanovaccines.[28]

Herein, we used model antigen ovalbumin (OVA) as the protein template for Bi_2S_3 nanoparticles synthesis, showing a high loading capacity of antigens. Synthesized Bi_2S_3@OVA NPs were loaded on DCs to construct Bi_2S_3@OVA@DC vaccines, which can introduce strong immune responses compared to DCs pulsed with free OVA, shown as an increase in phenotypic DC maturation markers, $CD4^+/CD8^+$ T cell activation, and OVA-specific cytotoxic T lymphocytes (CTLs) response in vitro. Furthermore, owing to the inherent high X-ray absorption and easy labeling performance of Bi_2S_3@OVA NPs, Bi_2S_3@OVA@DC exhibits a rapid and sustained accumulation in draining LNs, enabling the noninvasive tracking by CT imaging. Meanwhile, Bi_2S_3@OVA@DC delivered into the tumor coordinately facilitates the maturation of the tumor-associated DCs, which further increase the percentage of $CD8^+$ T cells and efficient response of OVA-specific IgG1/IgG2α antibody in the serum. Consequently, Bi_2S_3@OVA@DC achieves greater therapeutic effects against established OVA-expressing B16F10-OVA melanoma by preferably enhancing the infiltration of CTLs and decreasing the percentage of Treg cells in tumors, especially when combined with fractionated radiotherapy.

2 | RESULTS AND DISCUSSION

2.1 | Characterization and intracellular kinetics of Bi_2S_3@OVA@DC

This work aimed to develop nanoparticle preloaded dendritic cells (DCs) as an enhanced type of cell vaccine used for immunotherapy and the preparation procedure was schematically shown in Figure 1A. To this end, we first synthesized Bi_2S_3@OVA nanoparticles (NPs) using $Bi(NO_3)_3$ and chicken albumin with thioacetamide (TAA) as the sulfur source. The morphology of Bi_2S_3@OVA NPs was spheroid with filaments and the resulting spheroid size of NPs was 10 ± 2.1 nm by TEM (Figure 1B). The hydrodynamic diameter of the Bi_2S_3@OVA NPs was 165.2 ± 0.8 nm (Figure 1C). In general, the morphology of the NPs in the TEM images showed an area of the nanoparticles in a dry state with a high density of electron absorption, while DLS is the size of NPs in the aqueous solution. The large number of proteins available in the NPs may lead to the large size difference between the TEM and DLS results. NPs were stably dispersed in water, PBS and DMEM containing 10% FBS (Figure S1A) with negatively charged surfaces (–36.7 ± 0.6 mV in H_2O, Table S1). Compared to OVA alone, the UV-vis-NIR spectrum of Bi_2S_3@OVA NPs (red curve) showed a uniquely broad absorbance peak from 400 to 800 nm (Figure S1B). FT-IR spectrum of Bi_2S_3@OVA NPs appeared to be similar to that of OVA, indicating the presence of OVA in the NPs (Figure S1C). The chemical composition of Bi_2S_3@OVA was determined via XPS analysis (Figure 1D). The fitted spectrum of Bi 4f in Figure 1D containing two characteristic peaks (Bi 4f5/2, 158.74 eV and Bi 4f7/2, 163.11 eV) ascribed to the binding of Bi with S was observed. The elemental composition of the as-synthesized Bi_2S_3@OVA NPs was analyzed by elemental linear screening through energy-dispersive X-ray spectroscopy (EDX), shown with Bi as the major metal element in the NPs (Figure S2).

To generate DCs with high-quality, mouse bone marrow cells were induced by interleukin-4 and GM-CSF with a DCs phenotypic characterization of $CD11c^+$ $F4/80^-$ in flow cytometry. CCK8 assay showed no viability decrease in DCs with Bi_2S_3@OVA NPs concentration ranging from 2.5 to 200 μg/ml, indicating that the NPs were nontoxic to DCs (Figure S1D). The nontoxic concentration of NPs was used for incubation with cells to obtain NP preloaded DCs. Bi_2S_3@OVA were then labeled with Cy and showed a unique absorbance at 800 nm (Figure S3), aiming to localize NPs in DCs. After 2 h of incubation with Bi_2S_3@OVA-Cy, confocal microscopic images showed dotted fluorescence (red color) in the cytoplasm, suggesting an efficient cellular uptake of NPs by DCs (Figure 1E). Cell uptake of Bi_2S_3@OVA-Cy was rapid that the kinetics of cellular uptake of Bi_2S_3@OVA NPs showed a time-dependent increase in DCs (Figure 1F), with NP-positive cells at 62.7% within 2 h (Figure S4).

2.2 | Bi_2S_3@OVA NPs stimulate phenotypic maturation and antigen presentation of DCs

To explore the ability of Bi_2S_3@OVA NPs on DCs maturation in vitro, DCs were treated with endotoxin-free OVA

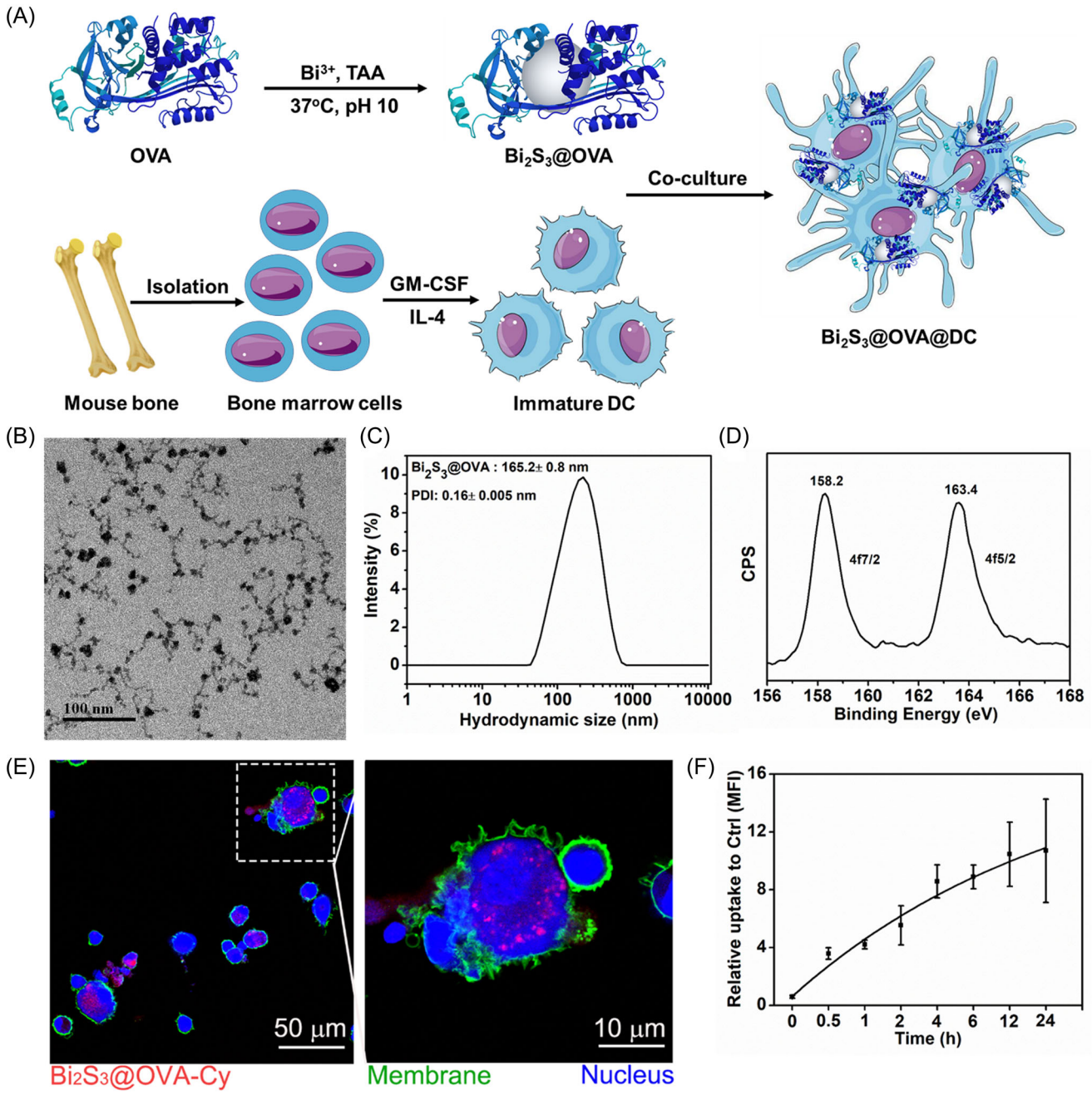

FIGURE 1 Characterization of Bi_2S_3@OVA@DC and cellular uptake kinetics. (A) Schematic illustration of Bi_2S_3@OVA@DC vaccines synthesis. (B) TEM images of the Bi_2S_3@OVA NPs. (C) DLS of Bi_2S_3@OVA in deionized water. (D) XPS spectrum for Bi_2S_3 nanoparticles 4f7/2 and 4f5/2. (E) Confocal images showing Bi_2S_3@OVA NPs endocytosis within 2 h. The cell membrane was stained with DiO (green), and the cell nucleus was stained with DAPI (blue). Nanoparticles were labeled with Cypate (red). (F) Cellular uptake kinetics of Bi_2S_3@OVA-Cy in bone marrow-derived dendritic cells (BMDC) as analyzed by flow cytometry ($n = 3$)

protein (a model antigen) or Bi_2S_3@OVA NPs at 5, 10, 20 μg/ml for 6 h, CD80 and CD86 were analyzed. The endotoxin level in Bi_2S_3@OVA NPs was tested by Gel Clot TAL Assay and demonstrated to be lower than 0.25 EU/ml in the Bi_2S_3@OVA NPs suspension (1 mg/ml). Compared to OVA that had minimal changes on phenotypic surface markers, Bi_2S_3@OVA at as low as 5 μg/ml (OVA) enhanced the expression levels of DCs maturation markers including CD80 (1.8-folds) and CD86 (1.5-folds) (Figures 2A and B; S5A and B for representative contour plots in the gating strategy of the flow cytometry), which may likely due to the adjuvant characteristic of Bi_2S_3 NPs. DC is a major type of professional APC that can take up tumor antigens, process the antigen proteins into a peptide, display the antigen epitope in the context of H-$2K^b$ (MHC I), interact with T cells, and initiate an antigen-specific immune response. We next investigated whether Bi_2S_3@OVA can enhance antigen presentation. Here, DCs were treated with free OVA antigen or Bi_2S_3@OVA, followed by antibody staining for the OVA epitope in the context of H-$2K^b$. OVA-treated DCs showed an extremely low level of OVA epitope that was comparable to nontreated DCs (Figure 2C). By contrast, Bi_2S_3@OVA treatment on DCs introduced a higher expression of SIINFEKL/H-$2K^b$ (5 μg/ml, 1.2-folds; 10 μg/ml, 1.5-folds) in a concentration-dependent manner. Compared with the control, the Bi_2S_3@OVA ($p < 0.01$) exhibited a

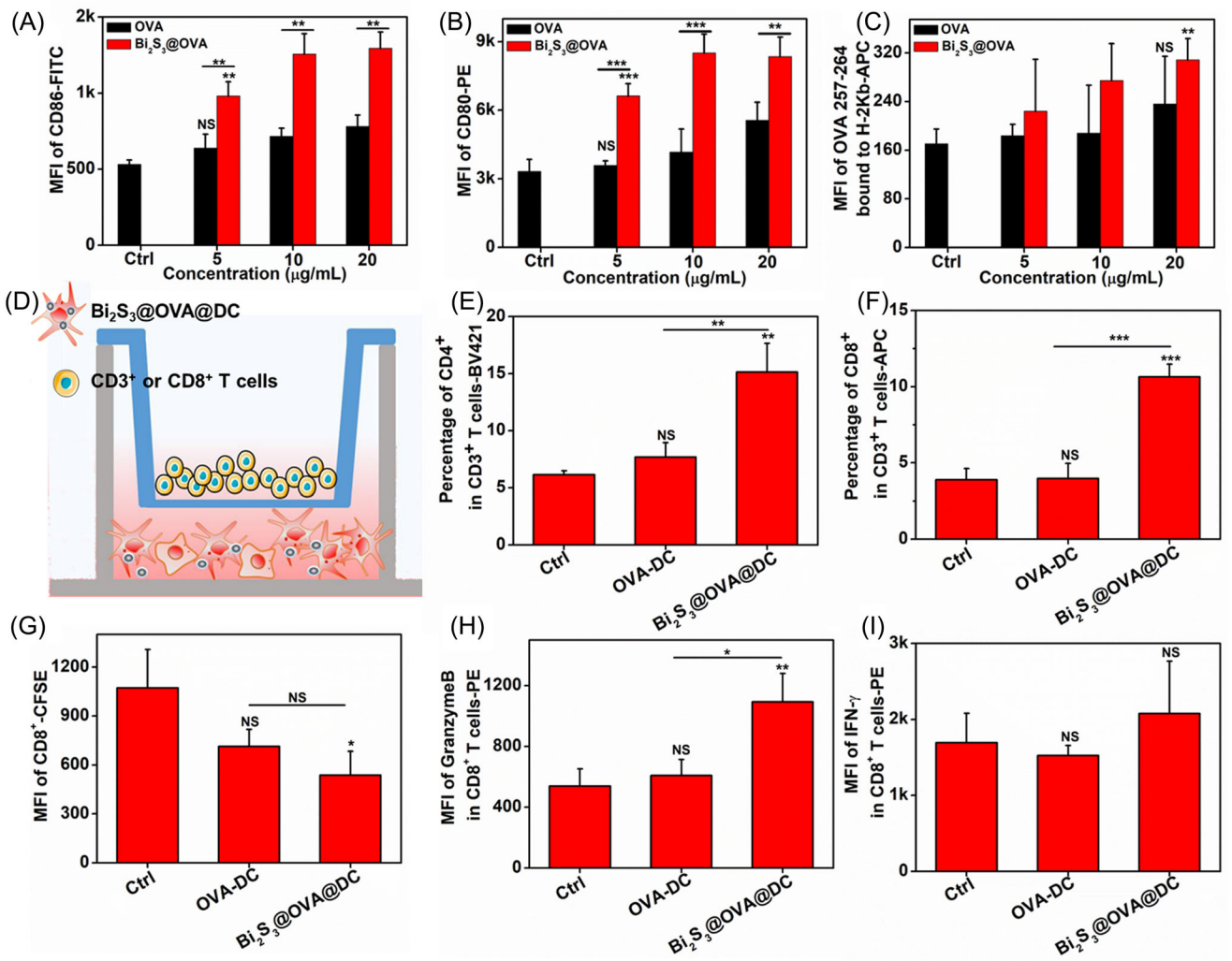

FIGURE 2 BMDC maturation by Bi_2S_3@OVA NPs and activation of T cells in vitro by Bi_2S_3@OVA@DC. (A–C) Phenotypic marker quantification of BMDC. BMDC were incubated with OVA or Bi_2S_3@OVA NPs for 6 h and stained by antibodies for surface markers of DCs (A, representative column chart for a percentage of $CD11c^+/F4/80^-/CD80^+$; B, mean fluorescence intensity [MFI] of $CD11c^+/F4/80^-/CD86^+$). (C) The antigen display of BMDC specific for OVA257-264 on H-$2K^b$. (D) Schematic illustration of activation of T cells by Bi_2S_3@OVA@DC in the transwell coculture system. $CD3^+$ T or $CD8^+$ T cells (in the upper chamber) isolated from the spleen of male C57BL/6J mice were stained with CFSE and cocultured with OVA-DC or Bi_2S_3@OVA@DC (in the under chamber) at 10 μg/ml. T-cell proliferation was evaluated by flow cytometry 4 days later. Percentage of $CD4^+$ T (E) or $CD8^+$ T (F) cells in $CD3^+$ T cells from splenocytes. The activation presented by CFSE-labeled cell proliferation (G) and cytotoxic effect of the $CD8^+$ T cells (Granzyme B expression) in splenocytes. (I) IFN-γ expression in $CD8^+$ T cells. Error bars represent mean ± SD ($n = 3$). p Values were calculated by one-way ANOVA. (NS: no significance, $^*p < 0.05$, $^{**}p < 0.01$, $^{***}p < 0.001$)

significant difference at 20 μg/ml concentration for OVA antigen processing but OVA alone had no difference. Thus, Bi_2S_3@OVA can induce the maturation of DCs by upregulating surface molecules (CD80, CD86) with efficient antigen presentation. With the increased interest in metalloimmunotherapy, researchers believe that metal ions can also play an important role through cell signal transduction in innate immunity.[29,30] Possibly Bi_2S_3 NPs can not only serve as an antigen carrier but also may exert in the metal adjuvants effect. As shown in Figure S6A, both OVA and Bi_2S_3@OVA inhibited the expression of cGAS protein in BMDCs (the quantification in Figure S6C), but surprisingly Bi_2S_3@OVA furtherly elevated the expression of interferon regulatory factor-3 (IRF-3) (the quantification Figure S6D), a downstream protein of STING signaling pathway induced by the STING's agonist 2'3'-cGAMP. Taken together, we believe that Bi_2S_3 NPs may play an adjuvant effect in amplification of the STING signaling and production of type I IFNs (schematic illustration shown in Figure S6B).

2.3 | Bi_2S_3@OVA@DC promote T-cell activation and proliferation

To determine whether Bi_2S_3@OVA@DC promotes T-cell activation, T-cell proliferation, and cytotoxic T-cell effect by $CD8^+$ T cells were displayed by coculturing T cells and Bi_2S_3@OVA@DC in a transwell format, which was schematically shown in Figure 2D. $CD3^+$ T or $CD8^+$ T cells (in the upper chamber) isolated from male C57BL/6J mice were prestained with 5(6)-carboxyfluorescein diacetate succinimidyl ester (CFSE), while the lower chamber contained OVA-DC or Bi_2S_3@OVA@DC that had been pretreated with OVA or Bi_2S_3@OVA NPs. T-cell proliferation was evaluated by flow cytometry 4 days later. We measured the percentage of $CD4^+$ (Figure 2E) and $CD8^+$ (Figure 2F) T-cell subsets in the $CD3^+$ T cells and found that the $CD3^+$ T cells coincubated with Bi_2S_3@OVA@DC activated $CD4^+$ and $CD8^+$ T cells with a significant level of threefold and 2.5-fold higher, respectively than the OVA-DC group. This study

suggests that the OVA-DC showed no statistical difference in the stimulation of T cells compared with the control group, while Bi_2S_3@OVA@DC NPs could efficiently stimulate the T-cell proliferation by delivering the model antigen OVA epitope peptide and adjuvant signal to the surface of T cells for their activation. It has been shown that mature and functional DCs release chemokines to attract T cells. In Figure S5C, we also directly coculture Bi_2S_3@OVA@DC vaccine with T cells at a cell density of 1:10 (nontranswell system). Our result demonstrated that the Bi_2S_3@OVA@DC vaccine can attract and interact with the surrounding T cells in vitro, thus activating the function of T cells. $CD8^+$ T-cell proliferation (Figure 2G) was the highest in the Bi_2S_3@OVA@DC sample, shown as reduced CFSE staining. Granzyme B belongs to a family of serine proteases expressed in the granules of cytotoxic T lymphocytes (CTLs) that can introduce apoptosis of malignant cells.[31,32] Our result showed a twofold increase of Granzyme B was detected in $CD8^+$ T cells by Bi_2S_3@OVA@DC vaccine compared to OVA pulsed DC (Figure 2H). IFN-γ is a representative cytokine secreted by helper T cells (Th1) that can activate T cells into the CTL subset,[33] and we found a slight increase in IFN-γ when cocultured with Bi_2S_3@OVA@DC vaccine but compared with control which had no significant different (Figures 2I and S5D). Therefore, we propose that the Bi_2S_3@OVA@DC is a high maturation form of a cell type that is capable of inducing Th1-cytokine secretion with a robust CTL-inducing effect.

2.4 | In vivo dLN targeted imaging and antigen-specific CTL responses

Timely and efficient delivery of vaccines to the secondary lymphoid system, for example, spleen and LNs, is essential for inducing strong and continuous immune responses against tumors.[34] Bismuth with an atomic number of 83 is one of the most promising contrast agents due to its high X-ray absorption rate.[35] It would be promising if the Bi_2S_3@OVA@DC vaccine can be tracked by CT imaging in vivo. This vaccine was injected from the footpad of mice and the axillary and inguinal LNs on the right side were illuminated with a higher CT signal (red dotted circle) (Figure 3A). Additionally, near-infrared (NIR) dye Cy was incorporated into Bi_2S_3 NPs allowing for real-time tracking of the migration of the LNs retention of the cell vaccine in vivo. NIR fluorescence imaging studies were carried out through subcutaneous administration of Bi_2S_3@OVA-Cy@DC into the foot paws of mice, with the Bi_2S_3@OVA-Cy serving as control (Figure 3B). The axillary and inguinal nodes of the mouse receiving Bi_2S_3@OVA-Cy@DC vaccines showed much stronger NIR fluorescence signals than those of the control, being retained for at least 24 h. As shown in Figure S7A and B, we quantified the CT value and NIR fluorescence intensity of the lymph nodes in the red dotted circle in Figure 3A and B. We also performed NIR I imaging and showed similar lymphatic homing effects of Bi_2S_3@OVA-Cy@DC and the cell vaccine was later metabolized by the liver and kidney 72 h later (Figure S7C). All in all, Bi_2S_3@OVA-Cy@DC have exhibited a rapid and sustained accumulation in LNs, enabling the noninvasive tracking by CT and NIR fluorescence imaging.

Owing to the immune memory effect of the lymphocytes trained by the cell vaccine, the memory T cells can be activated rapidly upon rechallenge.[36,37] Inspired by the efficient lymphatic homing and effective activation of $CD8^+$ T cells, we further evaluated the ability of Bi_2S_3@OVA@DC in generating OVA-specific CTLs response with the detailed procedures given in Figure 3C. Our results showed that subcutaneous immunization of mice with Bi_2S_3@OVA@DC introduced the highest level of splenocyte killing activity (Figure 3D). Immunization with Bi_2S_3@OVA@DC also induced the highest serum levels of OVA-specific Th1-related IgG2α (a 2.3-fold increase compared to control) and the Th2-related IgG1 (a 4.6-fold increase) (Figure 3E and F). Thus, we concluded that the Bi_2S_3@OVA@DC vaccine has great potential with an antitumor effect through CTLs and a balanced increase of antigen-specific IgG levels. The above results highly suggested that the Bi_2S_3@OVA-Cy@DC vaccine hold potential for providing long humoral and cellular immune responses.

2.5 | Determination of dose regimen for radiotherapy when combined with Bi_2S_3@OVA@DC

Radiotherapy can be delivered by standard, hypofractionated, and stereotactic ablative methods, while the radiation dose and fractionation strategy for optimal induction of antitumor immunity has not been fully revealed. By referring to previously reported segmentation methods,[38] we inoculated B16F10-OVA cells to establish the melanoma model, and then compared the antitumor effects and immune cell profile in the tumors among different radiation regimens (2 Gy × 6 or 6 Gy × 2 fractional therapy, or 12 Gy single dose) when combined with Bi_2S_3@OVA@DC. Due to the efficient targeting of Bi_2S_3@OVA@DC in the LNs, we subcutaneously administered Bi_2S_3@OVA@DC (100 μl/2 × 10^6 cells) on the back located on the contralateral side of the tumor for treatment, to initiate the treatment together with radiotherapy (experimental protocol shown in Figure 4A). In Figure 4B, all treatment groups have an inhibitory effect on the tumor growth compared to control, and the fractional radiotherapy (6 Gy × 2) combined with Bi_2S_3@OVA@DC obtained a maximal inhibition ($p < 0.0001$). The tumor growth curves of all individual mice are also shown in Figure S8. The body weights of all groups have no significant difference showing the safety of the cell vaccine (Figure S9). To profile the intratumor immune cells after the treatment, the tumors were digested and the percentage of mature DCs and T cells were quantified by flow cytometry. When combined with Bi_2S_3@OVA@DC, 6 Gy × 2 fractional radiotherapy showed a significantly higher percentage of mature DCs (Figure 4C and D) in tumors compared to 12 Gy dose ($CD11c^+/CD80^+$: 23.9% vs. 9.1%; $CD11c^+/CD86^+$: 37.6% vs. 11.4%) ($p < 0.05$). Radiotherapy alone showed a percentage increase of $CD4^+$ ($p < 0.05$) and $CD8^+$ ($p < 0.01$) T cells compared to control. It should be noted that when combined with Bi_2S_3@OVA@DC, radiotherapy showed a significant decrease in the percentage of $CD4^+$ T cells ($p < 0.001$) but an increase of $CD8^+$ T cells ($p < 0.001$) compared to radiotherapy alone (Figure 4E and F). It was suggested this difference may be because the Bi_2S_3@OVA@DC can inhibit the proportion of Treg

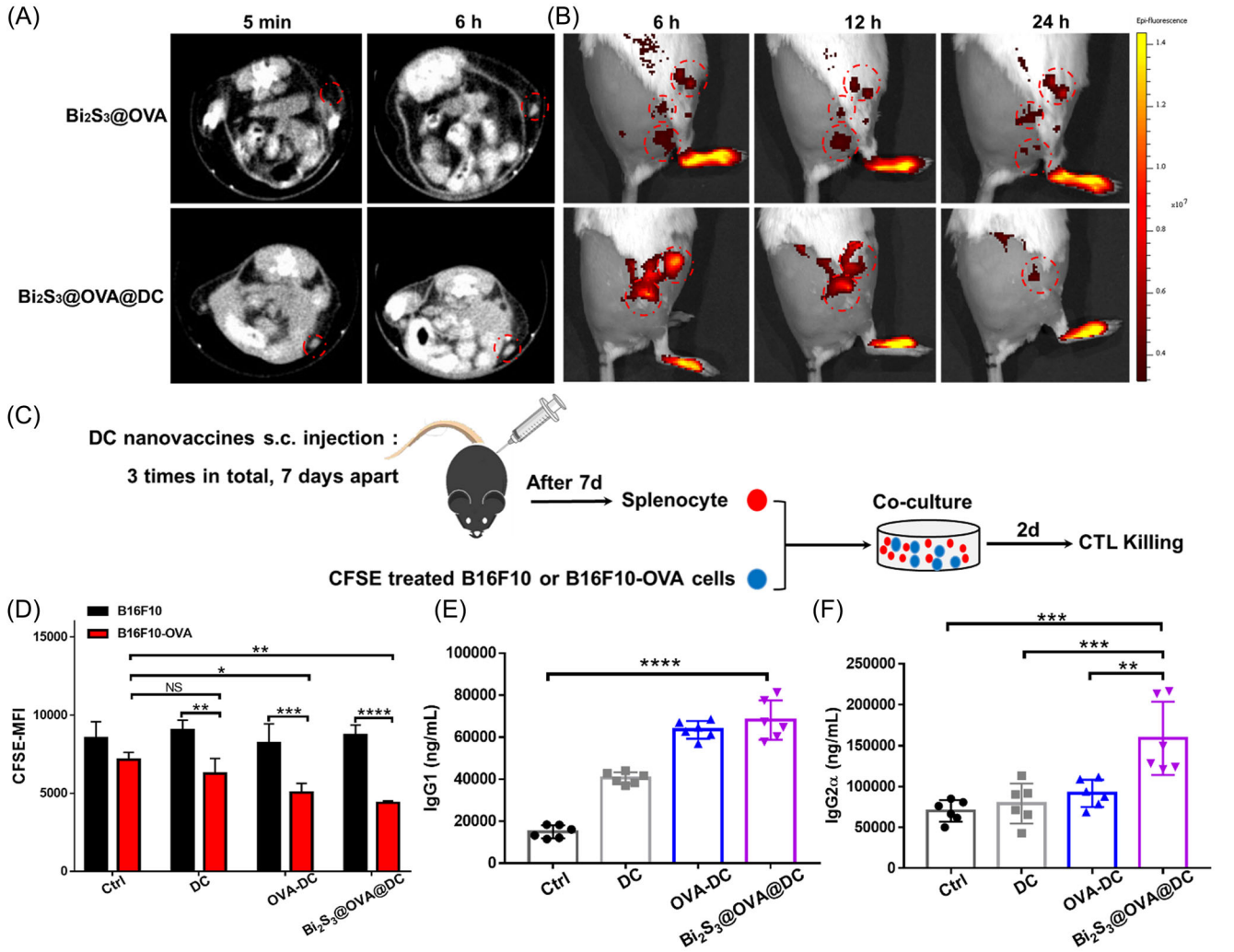

FIGURE 3 In vivo dLN targeted imaging and antigen-specific CTL responses of Bi_2S_3@OVA and Bi_2S_3@OVA@DC. Bi_2S_3@OVA-Cy (50 μl, 1 mg/ml) and Bi_2S_3@OVA-Cy@DC (50 μl, 2×10^6 cells) were injected into the mouse footpad respectively after 6, 12, and 24 h with NIR-II fluorescence and CT imaging. Representative tracing and accumulations in dLN by CT (A) and NIR-II fluorescence imaging (B). Inguinal LNs were shown by the red dotted circle. (C) Schematic illustration for the ability of Bi_2S_3@OVA@DC in generating OVA-specific CTL response. Mice were subcutaneously injected with DCs, OVA-DC, and Bi_2S_3@OVA@DC, respectively, three times. After 7 days of treatment, the spleen was collected for preparation of splenocyte suspension. The splenocytes in the pretreated mice were split in half and cocultured with CFSE-labeled B16F10 or B16F10-OVA. Two days later, the MFI of CFSE-labeled cells were quantified. (D) CTL response presented by CFSE-MFI in B16F10 and B16F10-OVA cells. OVA-specific IgG1 (E) or IgG2α (F) in the serum was quantified by ELISA ($n = 6$). p Values in C–E were calculated by one-way ANOVA. (NS: no significance, $^*p < 0.05$, $^{**}p < 0.01$, $^{***}p < 0.001$)

cells in $CD4^+$ T cells. Similarly, a combination of radiotherapy (including 2 Gy × 6, 6 Gy × 2 and 12 Gy) and Bi_2S_3@OVA@DC groups significantly increased the percentages of mature DCs in LNs than radiotherapy alone ($p < 0.05$, $p < 0.05$, $p < 0.01$, respectively) (Figure 4G and H). Interestingly, s.c. injection of Bi_2S_3@OVA@DC vaccines from the contralateral side of the tumor can also activate the DCs maturation in the LNs (Figure S10A and B) and the humoral immune system (Figure S10C and D) as well as an immune response in the spleen including an increase the percentage of mature DCs (Figure S11A and B) and T cells (Figure S11C and D).

As a result, we conclude that Bi_2S_3@OVA@DC specifically activated $CD8^+$ T cells in the tumors with a balanced increase of OVA-specific IgG level when synergized with radiotherapy, with a similar trend to the in vitro CTL response shown in Figure 3C–E. Our results also showed that Bi_2S_3@OVA@DC combined with a different fractional dose showed a similar increase in the proportion of antitumor immune cells and specific antibodies. It is widely recognized that fractionated, rather than single-dose radiotherapy, can induce immunogenic cell death (ICD) and play a role in the abscopal effects.[39–42] Meanwhile, to the clinical safety of radiotherapy and inaccessibility of stereotactic radiotherapy (SBRT), we determined a 6 Gy × 2 fractional dose regimen to combine with Bi_2S_3@OVA@DC, which may benefit the tumor-bearing mice from this therapeutic method concerning an optimized tumor growth suppressive ability and a desirable immune effect.

2.6 | Inhibition of tumor growth by fractional radiotherapy and Bi_2S_3@OVA@DC

Based upon the above investigation, we determined 6 Gy × 2 fractional radiotherapy as the optimal regimen to combine with Bi_2S_3@OVA@DC for more detailed studies. B16F10-OVA melanoma bearing mice ($n = 6$) were irradiated by 6 Gy of X-ray and 24 h later s.c. administered with Bi_2S_3@OVA@DC (100 μl/2×10^6 cells) on the contralateral

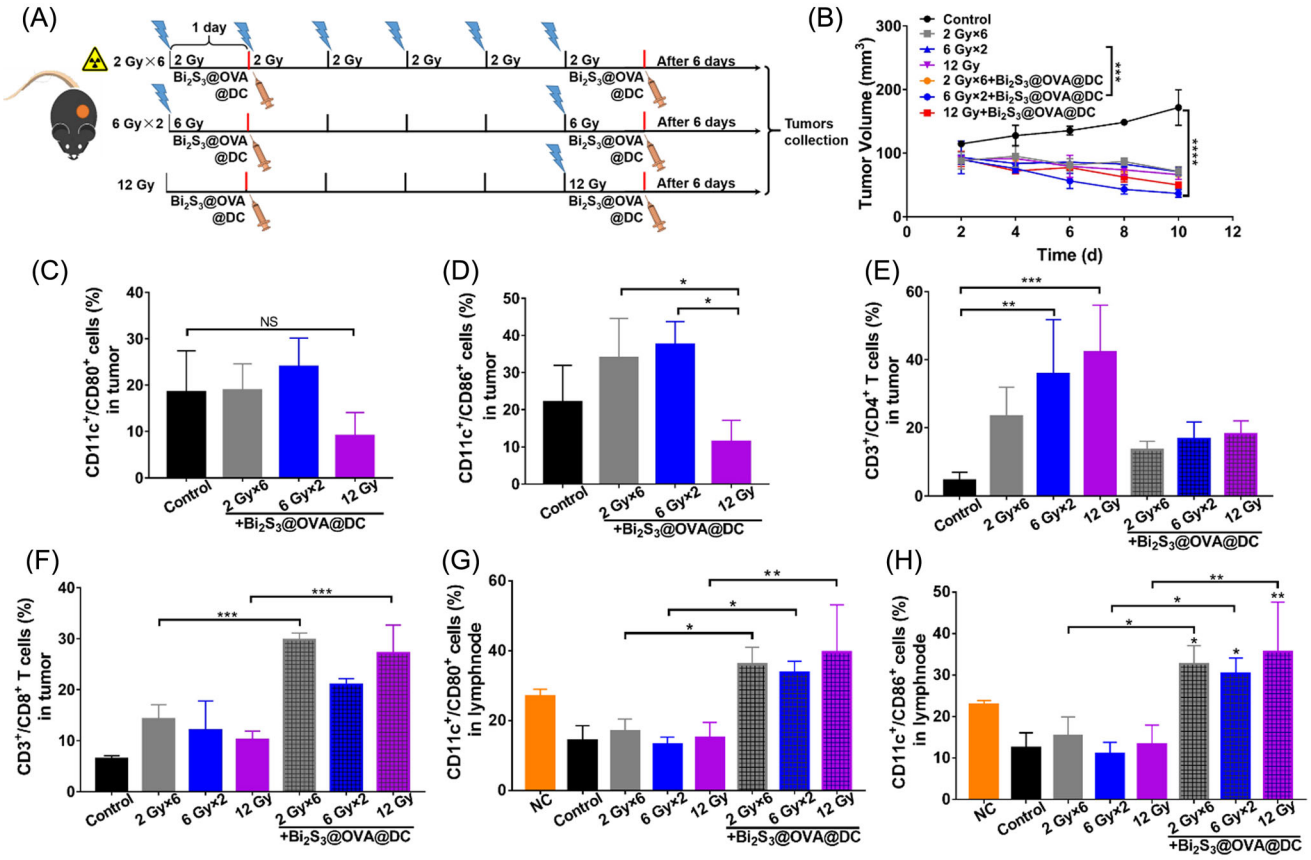

FIGURE 4 Dose regimen study for radiotherapy to suppress tumor growth when combined with Bi_2S_3@OVA@DC. (A) Schematic illustration of treatment protocols. C57BL/6J mice ($n = 6$ mice per treatment) were injected s.c. with B16F10-OVA (5×10^5 cells). When the tumor volume grew to 100 mm^3, mice received different radiotherapy (2 Gy × 6 or 6 Gy × 2 or 12 Gy) and injected s.c. with Bi_2S_3@OVA@DC (100 μl/2 × 10^6 cells). (B) Measurement of tumor volume by different treatments within 10 days. DCs maturation profile in tumors was determined by flow cytometry, presented by the percentage of $CD11c^+/CD80^+$ DCs (C) or $CD11c^+/CD86^+$ DCs (D). The percentage of $CD3^+/CD4^+$ T cells (E) or $CD3^+/CD8^+$ T cells (F) in tumors was also quantified. Additionally, the percentage of $CD11c^+/CD86^+$ DCs (G) or $CD11c^+/CD80^+$ DCs (H) in the dLNs was evaluated, where the negative control (NC) group was not inoculated with tumor cells. Error bars represent mean ± SD ($n = 6$). p Values were calculated by one-way ANOVA (NS: no significance, $*p < 0.05$, $**p < 0.01$, $***p < 0.001$)

side of the tumor. This procedure was repeated three times with a 6-day interval (Figure 5A). As shown in Figures 5B and S12 (the tumor growth curves of all individual mice), the tumors in the PBS group continued to grow at the highest growth rate. Similar to the results from the literature,[43–45] DC vaccines exhibited a certain level of the immune response against tumor growth, characterized by a weak tumor inhibitory effect, yet the tumor remain- massive in size 3 weeks later. In contrast, the tumor growth in mice irradiated with X-ray and immunized with Bi_2S_3@OVA@DC vaccine was remarkably suppressed with tumor size decreased by a factor of 82.5 compared to the control group. The tumor inhibitory effect of the X-ray+Bi_2S_3@OVA@DC may result from DCs maturation and the migration of cell vaccines to the lymphatic system, which consequently activate $CD8^+$ T cells or inhibit T regulatory cells, resulting in tumor inhibition. In this experiment, we first evaluated the maturation phenotype of DCs ($CD80^+/CD86^+$ in $CD11c^+$) in LNs (Figures 5C and S13). The percentage of mature DCs in the LNs markedly increased from 4% in the control group to 19% in the Bi_2S_3@OVA@DC vaccine or 33% in the combination group (X-ray+Bi_2S_3@OVA@DC). We then analyzed the percentage infiltration of $CD8^+$ T cells in the tumor and the results showed that the Bi_2S_3@OVA@DC vaccine alone significantly increased the percentage of $CD8^+$ T cells (15%) with approximately threefold higher than the nontreated group at 5.9% ($p < 0.05$), while the X-ray+Bi_2S_3@OVA@DC combination group exhibited the highest infiltration of $CD8^+$ T cells (32.4%) ($p < 0.001$) (Figure 5D). We also found that the percentage of Treg ($CD4^+/CD25^+/FOXP3^+$) cells in the X-ray group alone was significantly reduced compared to the control group (63.6% vs. 49%) ($p < 0.01$), while Treg was further reduced in the X-ray+Bi_2S_3@OVA@DC group (63.6% vs. 27%) ($p < 0.001$) (Figures 5E and S14). Therefore, we concluded that Bi_2S_3@OVA@DC vaccines can significantly activate DCs maturation in LNs and further activate the percentage of $CD8^+$ T cells and reduce Treg cells in vivo, which ultimately results in tumor inhibition when combined with X-ray irradiation.

Activated T cells are hyperresponsive resulting in upregulation of cytokine production (IFN-γ, TNF-α).[46] Our results showed that the cytokines IFN-γ (Figure 5F) and tumor necrosis factor-α (TNF-α) (Figure 5G) were significantly increased in the X-ray+Bi_2S_3@OVA@DC group compared to the control and the other treated group ($p < 0.001$). The body weights for these groups of mice were also recorded (Figure S15), with the mice in the treatment and control groups showing an inconspicuous difference in body weight for 3 weeks, which also indirectly proves that the DCs

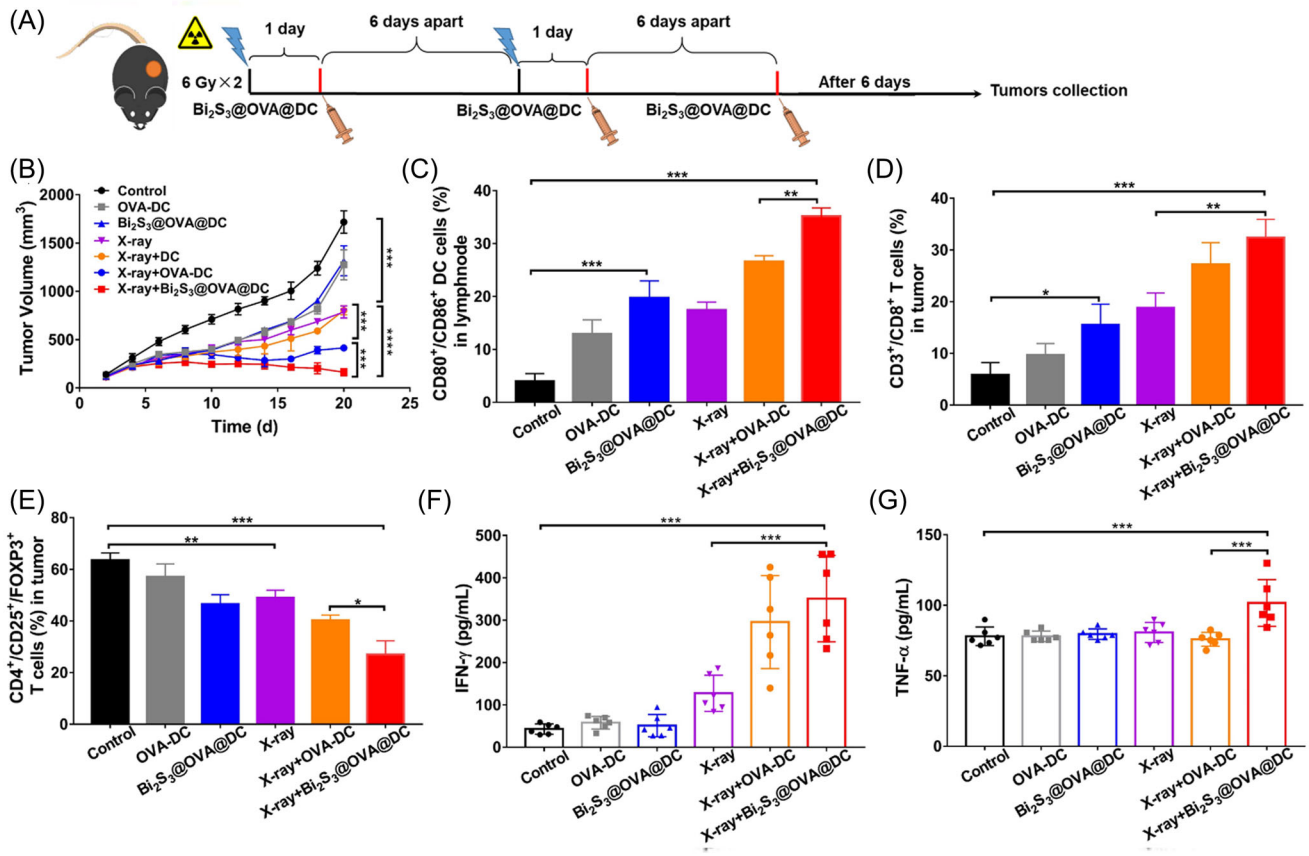

FIGURE 5 Inhibition of tumor growth by fractional radiotherapy and Bi_2S_3@OVA@DC. (A) Schematic illustration of fractional radiotherapy and Bi_2S_3@OVA@DC treatment protocols. (B) The tumor volume measurement during 21 days after tumor inoculation. (C) The percentage of $CD80^+/CD86^+$ mature DCs in LNs. (D) The percentage of $CD3^+/CD8^+$ T cells in tumors. (E) The percentage of Treg cells ($CD4^+/CD25^+/FOXP3^+$) in tumors. (F) INF-γ and (G) TNF-α cytokine levels detected by ELISA in serum from mice posttreatments. Error bars represent mean ± SD ($n = 6$). p Values in B–G were calculated by one-way ANOVA. (NS: no significance, $^*p < 0.05$, $^{**}p < 0.01$, $^{***}p < 0.001$). The statistically significant differences were only achieved at the endpoint

vaccines and fractional radiotherapy have minimal adverse effects on the health of the mouse model.

3 | CONCLUSION

In summary, we have designed and prepared a DC-based vaccine by engineering DCs with antigen-inspired Bi_2S_3 (Bi_2S_3@OVA@DC), which could arouse robust immunity against tumors when synergizing with radioimmunotherapy. Bi_2S_3@OVA@DC is a highly versatile vaccine platform that can be adapted to various personalized neoantigen peptides with efficient delivery to LNs with high specificity as well as the noninvasive visualization of DCs in vivo. Furthermore, the multifunctional Bi_2S_3@OVA@DC can support the highly modular and facile production of personalized neoantigen vaccines, guiding antigen processing and presentation by DCs to T cells, and triggering a strong antigen-specific immune response including enhanced T-cell proliferation, CTL-mediated responses, IFN-γ and balanced IgG1/IgG2α secretion in serum in immunized mice, showing remarkably improved efficiency compared to DCs pulsed by free antigen. In the meantime, the combination of Bi_2S_3@OVA NPs and STING agonists dramatically augmented STING activation; we believe that Bi_2S_3 NPs may play an adjuvant effect in amplification of the STING signaling. Comparing the common, organic-phase-synthesized nanoparticles whose antigen loading method is only by electrostatic adsorption,[47] Bi_2S_3@OVA NPs not only have better biocompatibility but also exhibit high whole-antigen loading efficiency. Our work is the first case of applying Bi_2S_3@OVA@DC in noninvasively trackable DCs-based immunotherapy, an approach with great in vivo tracking sensitivity and a highly efficient antigen-specific immune response, which are promising for future immunotherapy against major diseases including cancer. In addition, fractionated radiotherapy is one of the classic antitumor treatment methods and a preselected fractional regimen combined with DC vaccines will improve the tumor immune microenvironment status by inducing ICD. Thus, our treatment strategy through Bi_2S_3@OVA@DC combination with fractionated radiotherapy may have a meaningful impact on synergistic radioimmunotherapy for cancer and help promote the application of DC vaccines in clinic.

4 | EXPERIMENTAL SECTION/METHODS

4.1 | Synthesis and characterization of Bi_2S_3@OVA nanoparticles

OVA at 250 mg was added into the 250 ml round-bottomed flask diluted with 35 ml double-distilled water, and then 50 mM 5 ml $Bi(NO_3)_3$ were added. After stirring for 30 min at 37°C, 2 M 10 ml NaOH and 1 M 0.5 ml TAA were added and mixed. The reaction mixture was stirred at 37°C

for 12 h. Synthesized Bi_2S_3@OVA NPs were dialyzed for 24 h using an 8–15k MW dialysis membrane and 100k MW ultrafiltration tube to remove the free OVA. Bicinchoninic acid (BCA) assay (Beyotime Biotechnology) was used to quantify the OVA protein in Bi_2S_3 nanoparticles and ultrafiltrate followed by the calculation of the mass ratio of OVA: Bismuth = 3:1. To synthesize the Bi_2S_3@OVA-Cy based on the dye-induced assembly strategy of antigen molecule, 5 ml 20 mM cypate-NHS was added into 10 mg/ml Bi_2S_3@OVA NPs solutions and stirred for 24 h, and the solutions were dialyzed (8–15k MW) against ultrapure water for 48 h. All samples were observed using TEM at 120 kV (Tecnai G2 spirit BioTwin, FEI, USA). The core sizes of Bi_2S_3@OVA nanoparticles were analyzed using ImageJ. The hydrodynamic diameters were characterized using dynamic light scattering (DLS) (Malvern Instruments, UK). The surface charge was measured using a Zetasizer Nano-ZS90 (Malvern Instruments) instrument. Absorbance was measured using UV-vis absorbance spectroscopy (UV-3600, Shimadzu, Japan) and Fourier infrared spectrometer (NICOLET iS50, Thermofisher, USA). The concentration of bismuth on Bi_2S_3@OVA nanoparticles was measured by ICP-OES (ICAP7200, Thermofisher, USA). We obtained the X-ray photoelectron spectroscopy (XPS) (EXCALAB 250 XI, Thermo Scientific) spectra of the OVA conjugated bismuth nanoparticles.

4.2 | Bi_2S_3@OVA NPs stimulate phenotypic maturation and antigen presentation of DCs

The mouse bone marrow cells were obtained from the tibia and femur of C57BL/6J mice according to the established procedures. The cells were continuously cultured for 7 days in RPMI-1640 medium containing recombinant mouse granulocyte-macrophage cell clone stimulating factor (GM-CSF, Peprotech) and interleukin 4 (IL-4, BioLegend). Seven days later, the suspended and semisuspended cells were collected as differentiated DCs for subsequent experiments. To identify the maturity of DCs, differentiated DCs were incubated with 5, 10, 20 μg/ml OVA, Bi_2S_3@OVA for 24 h, followed by the cell wash with PBS and incubation with CD80/86 antibodies for 30 min. Cells were also stained with antibodies for BV421-CD11c, APC-F4/80, FITC-CD80, or PerCP/Cy5.5-CD86 for phenotype analysis using flow cytometry. Differentiated DCs were also treated with free OVA or NPs for 6 h and stained with BV421-CD11c and PE-OVA257-264 (SIINFEKL) peptide antibody to quantify OVA-specific epitope presentation on the surface of DCs using flow cytometry.

4.3 | Bi_2S_3@OVA@DC promote T-cell activation and proliferation

We use the transwell coculture system (with a pore size of 0.4 μm, Corning, USA) to investigate the activation of T cells by Bi_2S_3@OVA@DC. The $CD3^+$ T or $CD8^+$ T cells (in the upper chamber) isolated from male C57BL/6J mice were stained with 5 μM CFSE in 37 °C 20 min and cultured in RPMI medium with 0.1 % CD28 antibodies. The 5×10^5 CFSE-treated $CD3^+$ T or $CD8^+$ T cells cocultured with 5×10^4 OVA-DC or Bi_2S_3@OVA@DC (in the lower chamber) at 10 μg/ml for 4 days were detected by investigating T-cell activation by flow cytometry. T cells were collected and stained with BV421-CD4, FITC-CD8, PE-Granzyme B, and PE-IFN-γ antibodies for phenotype analysis using flow cytometry.

4.4 | Western blot assay

Cell lysates were loaded on SDS-PAGE gels and transferred to PVDF membranes. Indicated primary antibodies were incubated overnight at 4°C and HRP-linked Goat antirabbit IgG or antimouse IgG was used as the secondary antibody. The blot signals were visualized by ECL using the Multicolor fluorescence chemiluminescence imaging analysis system (FluorChem M, USA).

4.5 | In vivo CTL killing assay

C57BL/6J male mice were randomly grouped into control, DCs, OVA-DC, and Bi_2S_3@OVA@DC, which were s.c. subjected with 2×10^6 cells DCs or 100 μg OVA ($n = 3$ mice per group) on days 14, 7, and 0. One week after day 0, naïve C57BL/6J mice were killed, and spleens and serum of the immunized mouse were collected. The spleens were mechanically disrupted, passed through 70 μm cell strainers and flushed with cold PBS. Single-cell suspension was pelleted and resuspended with lysis buffer to remove red blood cells and splenocytes were recovered in a complete medium. The B16F10 and OVA peptide overexpressed B16F10-OVA cells were labeled with 0.5 μM (low) or 5 μM (high) CFSE, respectively, in serum-free medium for 1 h in 37 °C. About 1×10^7 splenocytes were added to the 6-well plate, mixed with 1×10^5 CFSE (high) cells, and cultured for 48 h. After incubation, 1×10^5 CFSE (low) cells were added to each well as an internal control, resuspended in 300 μl staining buffer at 1000 rpm/5 min, and then detected by flow cytometry.

4.6 | Lymph nodes tracing of vaccines

2×10^6 cells differentiated DCs were preincubated with 1 mg/ml Bi_2S_3@OVA for 12 h, collected by centrifugation, and washed with PBS. Each C57BL/6J mouse with 8–10 weeks of age was injected s.c. with Bi_2S_3@OVA@DC (50 μl, 2×10^6 cells) or Bi_2S_3@OVA (50 μl, 1 mg/ml) through the left food pad. Mice were imaged and analyzed by in vivo imaging system (IVIS Spectrum, PerkinElmer) at 6, 12, 24, and 72 h. In addition, the same mice were imaged using a U-SPECT+/CT imaging system (MILABS) at 6 h.

4.7 | Determination of dose regimen for radiotherapy when combined with Bi_2S_3@OVA@DC

Male C57BL/6J mice (6–8 weeks old) were inoculated s.c. with 5×10^5 B16F10-OVA cells in the flank on day 5 and were treated when the tumor volume reached 100 mm^3. The tumor site was irradiated with single and fractionated

irradiation, with specific programs at 2 Gy × 6 (from days 2 to 7, sequential), 6 Gy × 2 (on days 2 and 7) and single-dose 12 Gy on day 7, while Bi_2S_3@OVA@DC vaccines were given on days 3 and 8 for a total of 2 doses. All irradiation was performed using the biological X-ray radiation research platform (Rad source, RS-2000 Pro, USA). Six days after the treatment, the mice were sacrificed by humanitarian methods, and the tumors, spleen, and LNs of the mice were collected to evaluate the therapeutic effect and immune cell infiltration. Perpendicular tumor diameters were measured using calipers. Volume was calculated using the formula $L \times W^2 \times 0.52$, where L is the longest dimension and W is the perpendicular dimension. IgG1 and IgG2α levels in serum were detected by ELISA kits.

4.8 | Inhibition of tumor growth by fractional radiotherapy and DC-based vaccines

To evaluate the antitumor efficacy of Bi_2S_3@OVA@DC vaccines, B16F10-OVA tumor-bearing C57BL/6J mice were treated as the following: (1) control group (100 μl PBS), (2) OVA-DC (100 μl/2 × 10^6 cells), (3) Bi_2S_3@OVA@DC (100 μl/2 × 10^6 cells), (4) X-ray, (5) X-ray+ DCs (100 μl/2 × 10^6 cells), (6) X-ray+ OVA-DC, (7) X-ray+ Bi_2S_3@OVA@DC. X-ray radiation was performed at a dose of 6 Gy × 2 (on days 2 and 8) (Rad Source, RS-2000 Pro, USA). During the treatment, the weights and tumor volumes of mice were measured every other day. Tumor volume was calculated as the following: Volume was calculated using the formula $L \times W^2 \times 0.52$. The tumors, spleen and LNs were collected for flow cytometric analysis, and serums were collected and diluted for analysis. TNF-α and IFN-γ were analyzed with the corresponding ELISA Kits (Lianke Biotech, Hangzhou, China) according to the manufacturer's protocols.

4.9 | Flow cytometry

For flow cytometric analysis of in vivo experiments, tumor, spleen, and LNs were harvested 6 days after tumor treatment. Single-cell suspensions were prepared and red blood cells were lysed using ACK Lysis Buffer (Beyotime Biotechnology). Cell surface staining was performed using antibodies. In the gating strategy of the flow cytometry, T-cell phenotype was defined by $CD3^+/CD8^+$ or $CD3^+/CD4^+$ double positive, CTL cells as $CD8^+$/Granzyme B^+ or $CD8^+$/IFN-γ^+ double positive phenotype, mature DCs as $CD11c^+$/F4-80^-/$CD80^+$/$CD86^+$ phenotype, and regulatory T cells (Tregs) as $CD4^+/CD25^+/FOXP3^+$ triple positive phenotype. FACSVerse (BD Biosciences) or FC500 (Beckman Coulter) with FlowJo version 10 (TreeStar) were used for flow cytometry analysis. See materials for a list of antibodies used.

4.10 | Statistical analysis

All data were expressed as mean ± SD. The significance of the difference between mean values was analyzed by one-way ANOVA and a probability value of $p < 0.05$ was considered statistically significant. $^*p < 0.05$, $^{**}p < 0.01$, $^{***}p < 0.001$.

ACKNOWLEDGMENTS

This work was supported by the National Natural Science Foundation of China (22122407, 12175162, 32171403, 12075164, 31971319, 21874097), National Key Research Program of China (2018YFA0208800), Tang Scholar Program, the Scientific Research Program for Young Talents of China National Nuclear Corporation and A Priority Academic Program Development of Jiangsu Higher Education Institutions (PAPD).

CONFLICT OF INTEREST

The authors declare no conflict of interest.

DATA AVAILABILITY STATEMENT

The data that support the findings of this study are available from the corresponding author upon reasonable request.

ORCID

Yong Wang https://orcid.org/0000-0003-4061-7956

REFERENCES

1. O. J. Finn, *Nat. Rev. Immunol.* **2018**, *18*, 183.
2. S. K. Wculek, F. J. Cueto, A. M. Mujal, I. Melero, M. F. Krummel, D. Sancho, *Nat. Rev. Immunol.* **2020**, *20*, 7.
3. Z. Hu, P. A. Ott, C. J. Wu, *Nat. Rev. Immunol.* **2018**, *18*, 168.
4. O. Demaria, S. Cornen, M. Daëron, Y. Morel, R. Medzhitov, E. Vivier, *Nature* **2019**, *574*, 45.
5. https://clinicaltrials.gov/ct2/show/NCT00779402
6. T. M. Beer, P. F. Schellhammer, J. M. Corman, L. M. Glode, S. J. Hall, J. B. Whitmore, M. W. Frohlich, D. F. Penson, *Urology* **2013**, *82*, 410.
7. A. Harari, M. Graciotti, M. Bassani-Sternberg, L. E. Kandalaft, *Nat. Rev. Drug Discov.* **2020**, *19*, 635.
8. T. J. Moyer, Y. Kato, W. Abraham, J. Y. H. Chang, D. W. Kulp, N. Watson, H. L. Turner, S. Menis, R. K. Abbott, J. N. Bhiman, M. B. Melo, H. A. Simon, S. Herrera-De la Mata, S. Liang, G. Seumois, Y. Agarwal, N. Li, D. R. Burton, A. B. Ward, W. R. Schief, S. Crotty, D. J. Irvine, *Nat. Med.* **2020**, *26*, 430.
9. R. S. Riley, C. H. June, R. Langer, M. J. Mitchell, *Nat. Rev. Drug Discov.* **2019**, *18*, 175.
10. H. Wang, D. J. Mooney, *Nat. Mater.* **2018**, *17*, 761.
11. D. J. Irvine, E. L. Dane, *Nat. Rev. Immunol.* **2020**, *20*, 321.
12. R. van der Meel, E. Sulheim, Y. Shi, F. Kiessling, W. J. M. Mulder, T. Lammers, *Nat. Nanotechnol.* **2019**, *14*, 1007.
13. H. Liu, K. D. Moynihan, Y. Zheng, G. L. Szeto, A. V. Li, B. Huang, D. S. Van Egeren, C. Park, D. J. Irvine, *Nature* **2014**, *507*, 519.
14. J. Conniot, A. Scomparin, C. Peres, E. Yeini, S. Pozzi, A. I. Matos, R. Kleiner, L. I. F. Moura, E. Zupančič, A. S. Viana, H. Doron, P. M. P. Gois, N. Erez, S. Jung, R. Satchi-Fainaro, H. F. Florindo, *Nat. Nanotechnol.* **2019**, *14*, 891.
15. Y. Wang, S. Lin, H. Jiang, Y. Gu, Y. Wu, J. Ma, Y. Ke, L. W. Zhang, Y. Wang, M. Gao, *CCS Chem.* **2021**, *3*, 1328.
16. R. Kuai, L. J. Ochyl, K. S. Bahjat, A. Schwendeman, J. J. Moon, *Nat. Mater.* **2017**, *16*, 489.
17. L. Scheetz, P. Kadiyala, X. Sun, S. Son, A. Hassani Najafabadi, M. Aikins, P. R. Lowenstein, A. Schwendeman, M. G. Castro, *J. J. Moon, Clin. Cancer Res.* **2020**, *26*, 4369.
18. A. Schudel, D. M. Francis, S. N. Thomas, *Nat. Rev. Mater.* **2019**, *4*, 415.
19. Y.-N. Zhang, J. Lazarovits, W. Poon, B. Ouyang, L. N. M. Nguyen, B. R. Kingston, W. C. W. Chan, *Nano Lett.* **2019**, *19*, 7226.
20. C. R. Perez, M. De Palma, *Nat. Commun.* **2019**, *10*, 5408.
21. Y. Kim, S. Kang, H. Shin, T. Kim, B. Yu, J. Kim, D. Yoo, S. Jon, *Angew. Chem. Int. Ed.* **2020**, *59*, 14628.
22. W. Katagiri, J. H. Lee, M.-A. Tétrault, H. Kang, S. Jeong, C. L. Evans, S. Yokomizo, S. Santos, C. Jones, S. Hu, G. E. Fakhri, K. Tsukada, H. S. Choi, S. Kashiwagi, *Adv. Healthcare Mater.* **2019**, *8*, 1900035.
23. J. D. Martin, H. Cabral, T. Stylianopoulos, R. K. Jain, *Nat. Rev. Clin. Oncol.* **2020**, *17*, 251.
24. P. Zhang, Y. Zhai, Y. Cai, Y. Zhao, Y. Li, *Adv. Mater.* **2019**, *31*, 1904156.
25. O. Martinez, J. Sosabowski, J. Maher, S. Papa, *J. Nucl. Med.* **2019**, *60*, 730.

26. R. Meir, K. Shamalov, O. Betzer, M. Motiei, M. Horovitz-Fried, R. Yehuda, A. Popovtzer, R. Popovtzer, C. J. Cohen, *ACS Nano* **2015**, *9*, 6363.
27. Y. Wang, Y. Wu, Y. Liu, J. Shen, L. Lv, L. Li, L. Yang, J. Zeng, Y. Wang, L. W. Zhang, Z. Li, M. Gao, Z. Chai, *Adv. Funct. Mater.* **2016**, *26*, 5335.
28. J. Zhou, A. V. Kroll, M. Holay, R. H. Fang, L. Zhang, *Adv. Mater.* **2020**, *32*, 1901255.
29. X. Sun, Y. Zhang, J. Li, K. S. Park, K. Han, X. Zhou, Y. Xu, J. Nam, J. Xu, X. Shi, L. Wei, Y. L. Lei, J. J. Moon, *Nat. Nanotechnol.* **2021**, *16*, 1260
30. M. Lv, M. Chen, R. Zhang, W. Zhang, C. Wang, Y. Zhang, X. Wei, Y. Guan, J. Liu, K. J. C. R. Feng. *Cell Res.* **2020**, *30*, 966.
31. B. M. Larimer, E. Wehrenberg-Klee, F. Dubois, A. Mehta, T. Kalomeris, K. Flaherty, G. Boland, U. Mahmood, *Cancer Res.* **2017**, *77*, 2318.
32. N. Anh, A. Ramesh, S. Kumar, D. Nandi, A. Brouillard, A. Wells, L. Pobezinsky, B. Osborne, A. A. Kulkarni, *Sci. Adv.* **2020**, *6*, eabc2777.
33. H. M. Gibson, B. N. McKnight, A. Malysa, G. Dyson, W. N. Wiesend, C. E. McCarthy, J. Reyes, W.-Z. Wei, N. T. Viola-Villegas, *Cancer Res.* **2018**, *78*, 5706.
34. J. De Vrieze, B. Louage, K. Deswarte, Z. Zhong, R. De Coen, S. Van Herck, L. Nuhn, C. Kaas Frich, A. N. Zelikin, S. Lienenklaus, N. N. Sanders, B. N. Lambrecht, S. A. David, B. G. De Geest, *Angew. Chem. Int. Ed.* **2019**, *58*, 15390.
35. W. Liao, P. Lei, J. Pan, C. Zhang, X. Sun, X. Zhang, C. Yu, S.-K. Sun, *Biomaterials* **2019**, *203*, 1.
36. L. Luo, M. Z. Iqbal, C. Liu, J. Xing, O. U. Akakuru, Q. Fang, Z. Li, Y. Dai, A. Li, Y. Guan, A. Wu, *Biomaterials* **2019**, *223*, 119464.
37. Q. Ni, F. Zhang, Y. Liu, Z. Wang, G. Yu, B. Liang, G. Niu, T. Su, G. Zhu, G. Lu, L. Zhang, X. Chen, *Sci. Adv.* **2020**, *6*, eaaw6071.
38. M. J. Frank, P. M. Reagan, N. L. Bartlett, L. I. Gordon, J. W. Friedberg, D. K. Czerwinski, S. R. Long, R. T. Hoppe, R. Janssen, A. F. Candia, R. L. Coffman, R. Levy, *Cancer Discov.* **2018**, *8*, 1258.
39. L. Hammerich, T. U. Marron, R. Upadhyay, J. Svensson-Arvelund, M. Dhainaut, S. Hussein, Y. Zhan, D. Ostrowski, M. Yellin, H. Marsh, A. M. Salazar, A. H. Rahman, B. D. Brown, M. Merad, J. D. Brody, *Nat. Med.* **2019**, *25*, 814.
40. Y. Min, K. C. Roche, S. Tian, M. J. Eblan, K. P. McKinnon, J. M. Caster, S. Chai, L. E. Herring, L. Zhang, T. Zhang, J. M. DeSimone, J. E. Tepper, B. G. Vincent, J. S. Serody, A. Z. Wang, *Nat. Nanotechnol.* **2017**, *12*, 877.
41. X. Lu, J. W. Horner, E. Paul, X. Shang, P. Troncoso, P. Deng, S. Jiang, Q. Chang, D. J. Spring, P. Sharma, J. A. Zebala, D. Y. Maeda, Y. A. Wang, R. A. DePinho, *Nature* **2017**, *543*, 728.
42. M. A. Miller, R. Chandra, M. F. Cuccarese, C. Pfirschke, C. Engblom, S. Stapleton, U. Adhikary, R. H. Kohler, J. F. Mohan, M. J. Pittet, R. Weissleder, *Sci. Transl. Med.* **2017**, *9*, eaal0225.
43. Y. Xia, Y. Xie, Z. Yu, H. Xiao, G. Jiang, X. Zhou, Y. Yang, X. Li, M. Zhao, L. Li, M. Zheng, S. Han, Z. Zong, X. Meng, H. Deng, H. Ye, Y. Fa, H. Wu, E. Oldfield, X. Hu, W. Liu, Y. Shi, Y. Zhang, *Cell* **2018**, *175*, 1059.
44. S. Liu, Q. Jiang, X. Zhao, R. Zhao, Y. Wang, Y. Wang, J. Liu, Y. Shang, S. Zhao, T. Wu, Y. Zhang, G. Nie, B. Ding, *Nat. Mater.* **2020**, *20*, 421.
45. S. Wang, L. Qin, G. Yamankurt, K. Skakuj, Z. Huang, P.-C. Chen, D. Dominguez, A. Lee, B. Zhang, C. A. Mirkin, *Proc. Natl. Acad. Sci. U.S.A.* **2019**, *116*, 10473.
46. N. Obermajer, J. Urban, E. Wieckowski, R. Muthuswamy, R. Ravindranathan, D. L. Bartlett, P. Kalinski, *Nat. Protoc.* **2018**, *13*, 335.
47. J. Xiang, L. Xu, H. Gong, W. Zhu, C. Wang, J. Xu, L. Feng, L. Cheng, R. Peng, Z. Liu, *ACS Nano.* **2015**, *9*, 6401.

SUPPORTING INFORMATION

Additional supporting information may be found in the online version of the article at the publisher's website.

How to cite this article: H. Yu, H. Guo, H. Zu, H. Ding, S. Lin, Y. Wang, L. W. Zhang, Y. Wang, *Aggregate* **2022**, e194. https://doi.org/10.1002/agt2.194